Electronic Supplementary Material (ESI) for Nanoscale.

Supporting Information :

Evolution of Ni nanofilaments and electromagnetic coupling in the resistive switching of NiO

Yuxiang Luo,[a,c] Diyang Zhao,[a,c] Yonggang Zhao,*[a,c] Fu-kuo Chiang,[b] Pengcheng Chen,[a,c] Minghua Guo,[a,c] Nannan Luo,[a,c] Xingli Jiang,[a,c] Peixian Miao,[a,c] Ying Sun,[a,c] Aitian Chen,[a,c] Zhu Lin,[a,c] Jianqi Li,*[b,c] Wenhui Duan,[a,c] Jianwang Cai,[b] and Yayu Wang,[a,c]

[a] Department of Physics and State Key Laboratory of Low-Dimensional Quantum Physics, Tsinghua University, Beijing 100084, China

[b] Beijing National Laboratory for Condensed Matter Physics, Chinese Academy of Sciences, Beijing 100190, China

[c] Collaborative Innovation Center of Quantum Matter, Beijing 100084, China

* To whom correspondence should be addressed: ygzhao@tsinghua.edu.cn; ljq@aphy.iphy.ac.cn

S1. Distinction between NiO and Ni structures

The crystal structure of NiO poly-crystalline film was resolved by the face-centered-cubic (fcc) NaCl structure with a lattice parameter of 4.178 Å ($Fm\bar{3}m$, space group No. 225) by means of electron diffraction patterns. Besides, the crystal structure of metallic Ni was also well defined as fcc structure ($Fm\bar{3}m$, space group No. 225) with a lattice parameter of 3.554 Å. The distinct facet d-spacing of NiO (111) (2.412 Å) and Ni (002) (1.777 Å) could be used to distinguish NiO and Ni structures under the real or reciprocal space without confusion.

S2. Multistep transition in the *I-V* curve for the SET and RESET processes

In both SET and RESET processes, multistep transitions can occur, just as shown in Figure S1. In the main text, we only take the RESET process as an example.

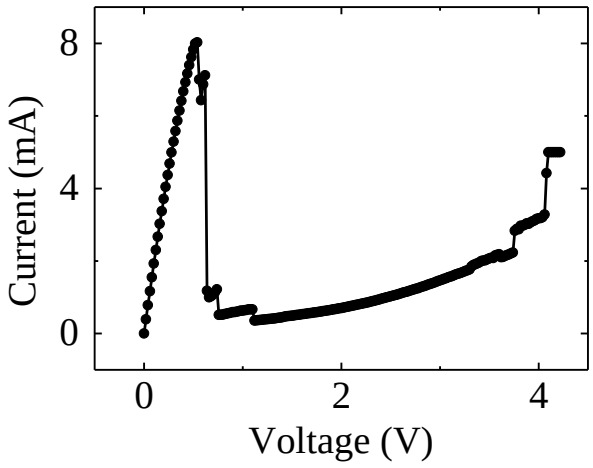

Figure S1. Multistep transition in the *I-V* curve for the SET and RESET processes

S3. Explanation of the three types of RESET processes in terms of Ni multi-nanofilaments

In the SET process, several Ni nanofilaments are formed and play the role of conducting paths between the top and bottom electrodes. It is expected that the LRS with a high conductance has nanofilaments with large thickness, so the difference of thickness among different nanofilaments is small compared to their thickness, which leads to almost concurrent rupture of all the nanofilaments (the type of sharp reset transition). In contrast, the LRS with a low conductance has nanofilaments with small thickness, so the difference of thickness among different nanofilaments is not small compared to their thickness, which leads to successive rupture of the nanofilaments (multistep reset transition).

S4. Temperature dependence of resistance curves for the LRS and the HRS with different resistances

The conclusion from the impedance spectra measurement is also revealed by the results of temperature dependence of resistance (*R*-*T*) for the LRS and the HRS with different resistances as shown in Figure S2. To begin with, the *R*-*T* curve of the LRS typically shows a weak metallic behavior (Figure S2a) and the relative resistance ratio (RRR), defined as R(300 K)/R(2 K), was found to be 1.75, which is much smaller than 47.4 of pure nickel metal,[1] possibly due to its low dimension. Moreover, the *R*-*T* curves of the HRS with different resistances show a transition from a weak metallic conduction to a semiconductor behavior as shown in Figure. S2b-f. For the HRS with resistances below hundreds of ohm, the sample shows a metallic conduction. While with the resistance value above tens of thousands of ohm,

the sample shows a semiconductor behavior with $R(T) \propto \exp(\phi_t / k_B T)$, where ϕ_t is the thermal activation energy and k_B is the Boltzmann constant. For the in-between resistances, *R-T* curves show a gradual transition from a metallic transport dominated by weak conductive filaments to semiconductor behavior. Multi-nanofilaments are involved in this phenomenon. In Figure S2c and S2d, the R-T curves are also used to prove this viewpoint. In these two figures, only some of the nanofilanments rupture. The ruptured filaments show the characteristic of an insulator, i. e. the resistance increases with decreasing temperature, with a small polaron hopping behavior.[2] While the unruptured filaments show a weak metallic behavior due to defects,[3] i. e. the resistance decreases with decreasing temperature. So weak metallic conduction and small polaron hopping coexist in the high-resistance off state with the former dominating at low temperatures and the latter dominating at high temperatures as shown in Figure S2c. In other words, when the temperature is higher than a cetain temperature (T_{th}), small polaron hopping dominates and the R-T curve shows the characteristic of an insulator. While below T_{th}, weak metallic conduction mainly works. It shows the characteristic of weak metallic behavior. For HRS with higher resistances, more defect are involved, localization effect due to defects becomes remarkable at low temperatures, so the resistance goes up again at low temperatures (Figure S2d). For HRS with much higher resistances, all Ni filaments rupture, the R-T curves just show the insulating behavior (Figure S2e,2f). Taking Figure S2c as an example, ln(R) vs $1/k_B T$ shows a positive slope above ~246 K with ϕ_t=12.98 meV, which is close to the value of 20 meV in the 300-nm-thick NiO thin film.[3]

From Figure S2b, we found that the RRR value is around 1.23 which is lower than 1.79 for the LRS, which can be attributed to the defective, impure metallic conducting nanofilaments.[4] This difference may be related with the different behaviors in the AMR for the LRS and HRS (Figure. 3b-d).

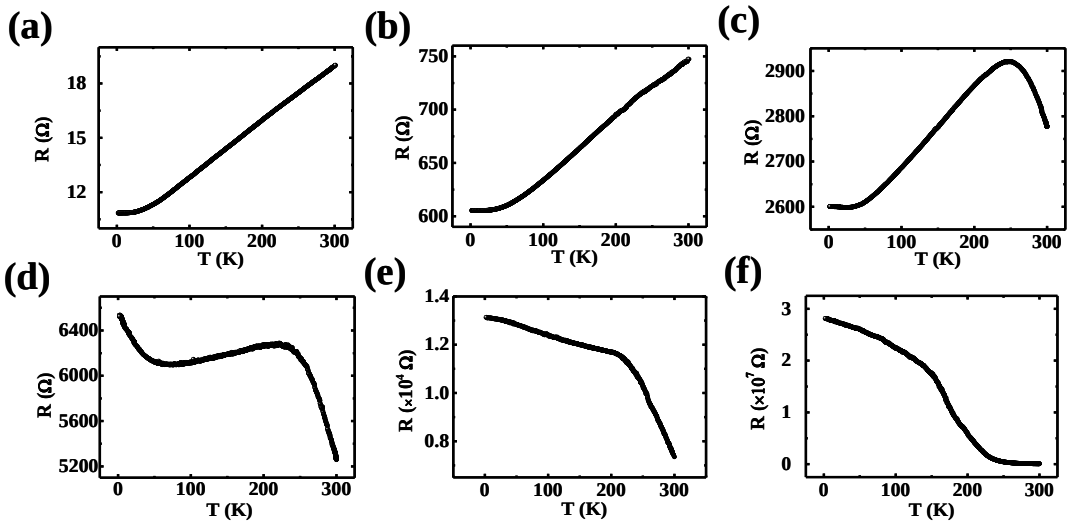

Figure S2. R-T curves for the LRS and the HRS with different resistances. (a) R-T curve for the LRS. (b)-(f) R-T curves for the HRS with different resistances.

S5. **The fitting curves along with the experimental data to get C_1**

Figure S3 shows the fitting curves along with the experimental data with six typical HRS with different resistance values. According to $(M'-a)^2+(M''-b)^2=R^2$, where R is the radius of M'-M'' semicircle and a, b are the coordinates of the circle center, we can get the value of a, b and R. So we can get the value of C_1 according to $C_0/C_1=2\times\sqrt{R^2-b^2}$ (here, C_0 is the capacitance when NiO is replaced by air and it is around 2.78×10^{-12} F) and the values of C_1 are shown in Figure 2e.

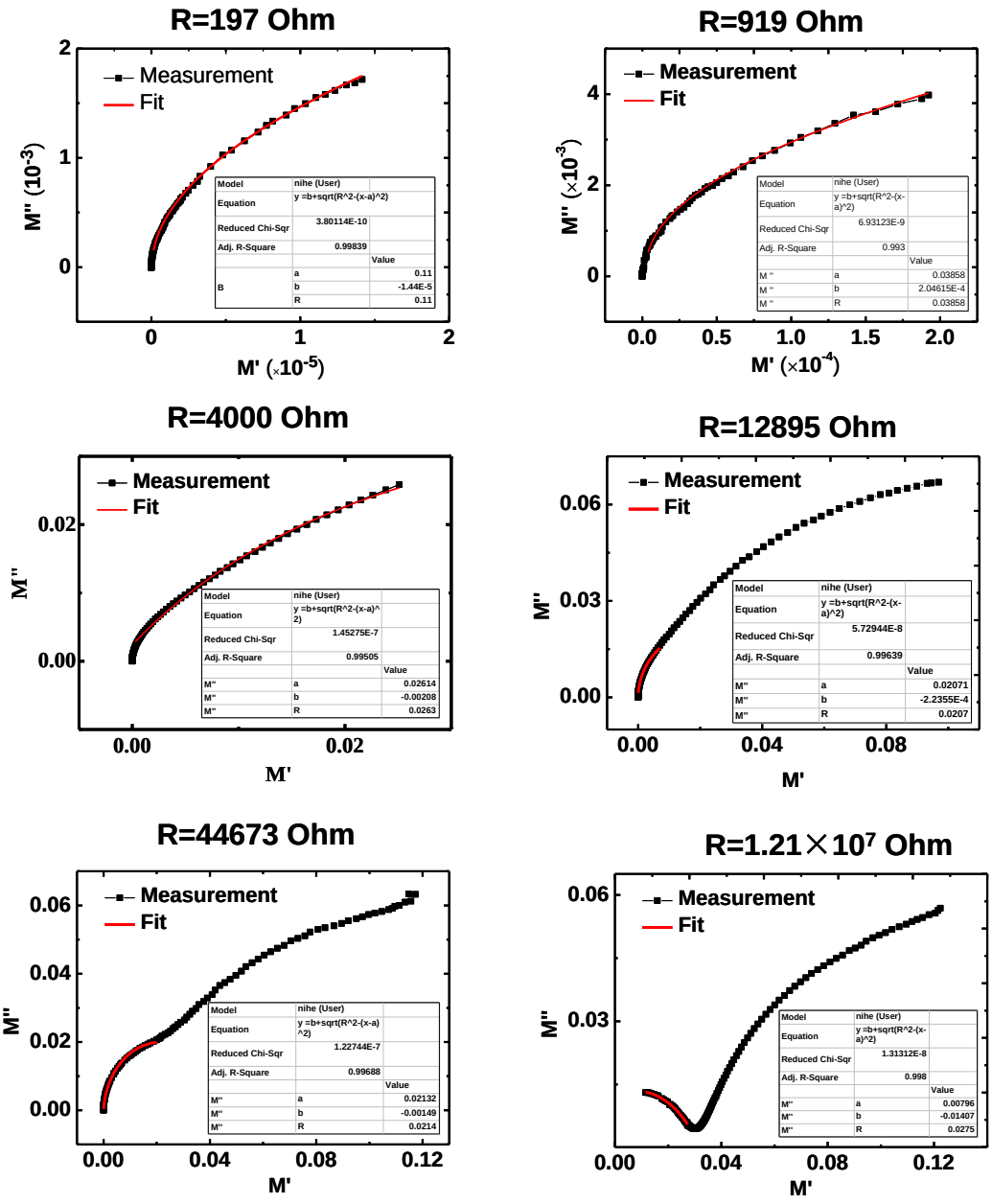

Figure S3 The fitting curves along with the experimental data

S6. S**tatistics of different reset behaviors for different compliance currents**

The compliance currents are 5mA (Figure S4(a)), 3mA (Figure S4(b)) and 1mA (Figure S4(c)), respectively. We measured 100 curves repetitively and made statistical analysis, just as shown in Figure S4. It is easy to find that the resistance of LRS is different in the same current compliance level. In detail, the sharp reset with black is mainly distributed in LRS

with low resistance, about 14 Ohm. The intermediate reset with red corresponds to around 20 Ohm. The multistep reset with blue correspond to around 29 Ohm. In the meanwhile，for smaller compliance current，the count of the LRS with high resistance increases. As a result, the count of I-V of multistep reset increases.

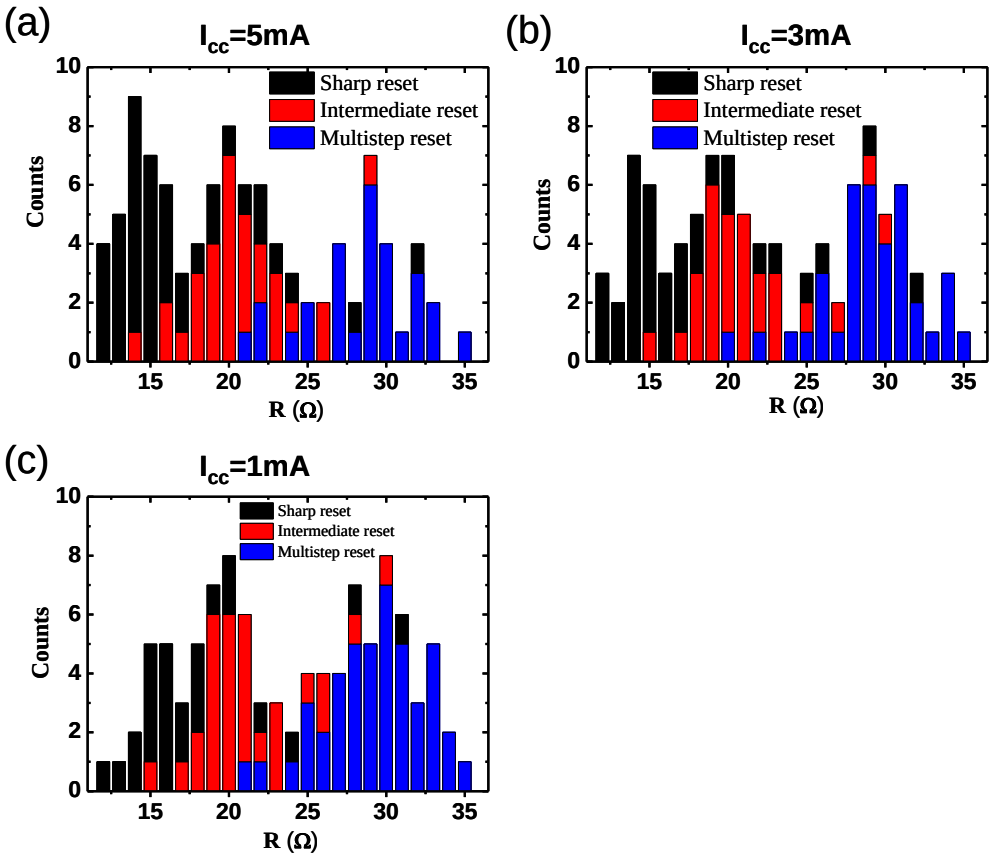

Figure S4. Sstatistics of different reset behaviors with compliance currents of 5mA, 3mA and 1mA, respectively.

S7. **Fitting data for R_1, R_2, C_1 and C_2 in the equivalent circuits of HRS in Figure 2c**

We give the fitting results of R_1, R_2, C_1 and C_2 in Figure. S5(a), (b) and (c) below. The fitting of R_1 and R_2 can only reach 3.63×10^4 Ohm. When the resistance is over 3.63×10^4 Ohm, there is a very small bump on the left of impedance spectra, which make it difficult to fit for R_1 and R_2. For the fitting of C_2, only when the resistance is over 3.63×10^4 Ohm, the

arc corresponding to C_2 can appear in the modulus data.

(a)

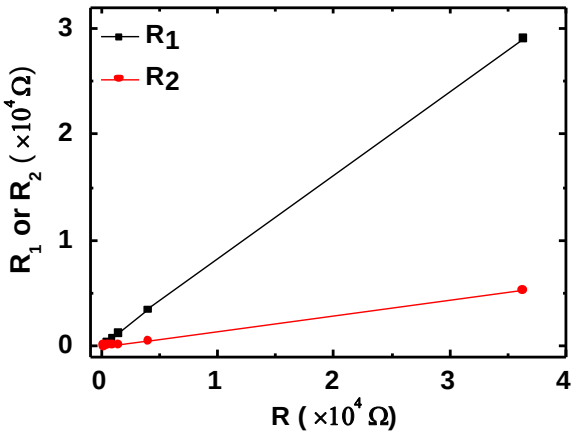

(b)

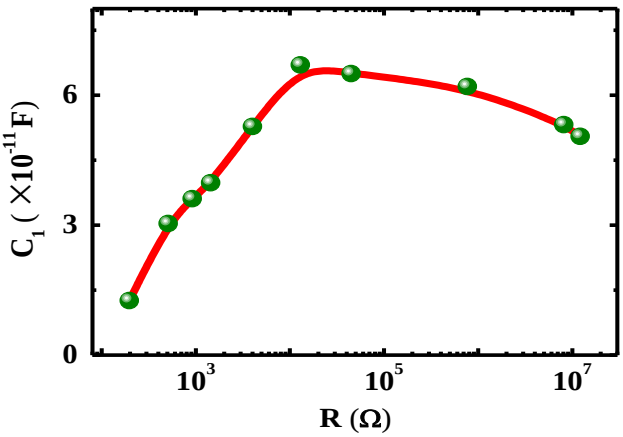

(c)

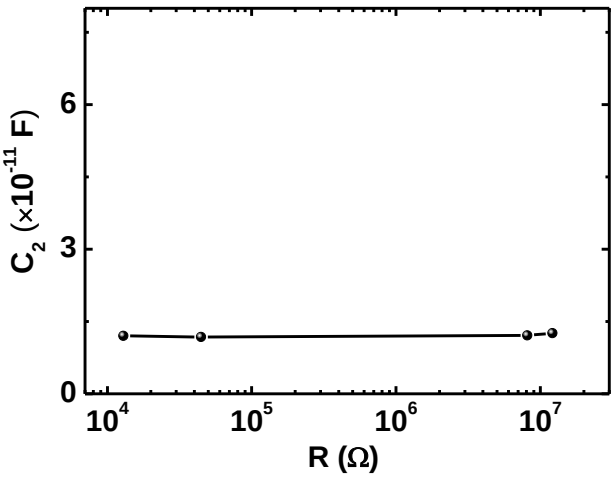

Figure S5 Fitting data for R_1, R_2, C_1 and C_2 in equivalent circuits of HRS

References

1 M. G. Kim, S. M. Kim, E. J. Choi, S. E. Moon, J. H. Park, C. Kim, B. H. Park, M. J. Lee, S. Seo, D. H. Seo, S. E. Ahn and I. K. Yoo, Jpn. *J. Appl. Phys.*, 2005, **44**, L1301.

2 P. Lunkenheimer, A. Loidl, C. R. Ottermann and K. Bange, *Phys. Rev. B*, 1991, **44**, 5927.

3 K. Jung, H. Seo, Y. Kim, H. Im, J. Hong, J. –W. Park and J. –K. Lee, *Appl. Phys. Lett.*, 2007, **90**, 052104.

4 R. Waser, R. Dittmann, G. Staikov and K. Szot, *Adv. Mater.*, 2009, **21**, 2632.